GPS Solutions (2023) 27:192
https://doi.org/10.1007/s10291-023-01532-3

ORIGINAL ARTICLE

Evaluation of real-time kinematic positioning performance of the BDS-3 PPP service on B2b signal

Peida Wu[1] · Yidong Lou[1] · Weixing Zhang[1] · Jan Dousa[2] · Huizhong He[4,5] · Junbing Chai[3] · Yongzhong Ouyang[4,5] · Zhenyi Zhang[1] · Xu Zou[1]

Received: 6 March 2023 / Accepted: 10 August 2023 / Published online: 25 August 2023

Abstract

The BeiDou global navigation satellite system (GNSS) of China (BDS-3) had full operation capacity on July 31, 2020, and started providing free precise point positioning (PPP) service on B2b signals. Although GNSS community has conducted many evaluations on the PPP-B2b products and its user performance, comprehensive evaluations of real-time PPP solutions using the BDS-3 PPP service at kinematic and highly kinematic platforms are still absent. We present a general evaluation of a real-time PPP performance exploiting the PPP-B2b corrections in various user situations represented with static stations, a car, an offshore vessel and an aircraft. We found that errors of the PPP-B2b corrections are less stable and higher approximately by a factor of two for GPS compared to BDS-3 medium earth orbit (MEO) satellites. An average convergence time of 28.5 and 12.9 min can be achieved with a standalone BDS-3 and BDS-3 + GPS solution for a low-speed object, such as a permanent station, a car, and a ship, in real time when using the PPP-B2b corrections. For a high-kinematic airborne platform, the convergence time is much longer, reaching 48.9 min. The 95% positioning errors after convergence are less than 20 and 35 cm in horizontal and vertical directions for all the experiments. We conclude that the PPP-B2b service offered by the BDS-3 is prospective for real-time kinematic positioning applications.

Keywords BDS-3 B2b · Real-time PPP · Positioning accuracy · Convergence time

Introduction

Precise point positioning (PPP) can achieve a decimeter-/centimeter-level positioning when using a single receiver. Hence, it has been widely used in scientific research and engineering applications, provided precise satellite orbit and clock products are available (Malys and Jensen 1990; Zumberge et al. 1997; Kouba and Héroux 2001). For real-time PPP users, the orbit and clock products can be obtained via the Internet (Internet-based PPP) or via a satellite link (Satellite-based PPP) (Xu et al. 2021). For the former, the precise products are generally sent to users using the Networked Transport of Radio Technical Commission for Maritime Services (RTCM) via Internet Protocol (NTRIP). An example is the Real-Time Service (RTS) launched by the International GNSS Service (IGS) in 2013 (Elsobeiey and Al-Harbi 2016; Hadas and Bosy 2015), whose quality has been continuously improving since that time. Currently, the accuracy of orbit products of GPS, GLONASS, Galileo, BDS3-MEO reaches a centimeter level, and the accuracy of clock corrections of GPS and Galileo is better than 0.2 ns while those of BDS and GLONASS is slightly worse (Li et al. 2022; Lou et al. 2022). Some typical products of the satellite-based real-time PPP service are provided by services such as the RTX of Trimble (Leandro et al. 2011), OmniStar (Booth and Snow 2009) and StarFire of NavCom (Dai et al. 2016); however, these commercial products are paid.

To meet the demands of a future potential market and for the convenience of professional users, some GNSS

✉ Yidong Lou
ydlou@whu.edu.cn

1 GNSS Research Center, Wuhan University, Wuhan 430079, China

2 Research Institute of Geodesy, Topography and Cartography, Zdiby 25066, Czech Republic

3 BGP Inc China National Petroleum Corporation, Zhuozhou 072751, China

4 Key Laboratory of Marine Environmental Survey Technology and Application, MNR, Beijing 100000, China

5 South China Sea Marine Survey Center, MNR, Beijing 100000, China

systems, including Galileo, Quasi-Zenith Satellite System (QZSS) and BeiDou system (BDS-3, hereafter referred BDS), have embedded the PPP service in the navigation system designs. On January 24, 2023, the Galileo authority started the delivery of an initial service of its free global High Accuracy Service (HAS) on the E6-B signal, targeting a 95% accuracy of 20 and 40 cm for real-time PPP horizontal and vertical positioning, respectively (European GNSS Service Center 2023). The new multi-GNSS advanced orbit and clock augmentation—precise point positioning (MADOCA-PPP) of QZSS launched a trial service on September 30, 2022, and planned to provide an operational service as of 2024 (Cabinet Office 2022). In July 2021, the BDS-3 announced the service supporting a kinematic decimeter-level and a static centimeter-level real-time PPP when using its GEO B2b signal (PPP-B2b) in China and surrounding areas.

Numerous studies have evaluated the performance of PPP-B2b products and user positioning. Tao et al. (2021) found that the differential code bias (DCB) of PPP-B2b shows a comparable performance with the DCB product provided by the University of the Chinese Academy of Sciences (CAS). Xu et al. (2021) evaluated the accuracy and availability of the PPP-B2b corrections for BDS. The results showed that the availability of PPP-B2b corrections in China was better than 80%, and the root mean square (RMS) errors of orbits were 6.8, 33.4 and 36.6 cm in radial, along-track and cross-track directions for the MEO satellites, whereas twice higher for the inclined geostationary orbit (IGSO) satellites, and the accuracy of clock offsets was about 0.2 ns. Zhang et al. (2022) compared the accuracy of the PPP-B2b corrections for BDS and GPS using 150 days in 2021. The results revealed that the RMS and standard deviation (STD) of the signal-in-space ranging error (SISRE) of GPS were almost double compared to BDS.

The performance of a static real-time PPP can achieve centimeter-level accuracy after a convergence (Liu et al. 2022; Ren et al. 2021). Xu et al. (2021) found that an accuracy of 11 cm horizontally and 17 cm vertically after convergence could be achieved for a kinematic PPP of a permanent station using B1C/B2a ionosphere-free (IF) combination and also discovered the B1C/B2a combination showed better accuracy than B1I/B3I. Zhang et al. (2022) demonstrated that a kinematic PPP of a car trajectory with PPP-B2b corrections achieved a position error of about 23.5 (18.6) and 48.8 (37.1) cm in the horizontal and vertical direction, respectively, with an average convergence time of 10.4 (14.2) min for a standalone BDS (BDS + GPS solution). Geng et al. (2022) found that a real-time PPP with the PPP-B2b service on a coastal area was characterized by a 3D error RMS of 21.3 cm for BDS and 18.2 cm for GPS + BDS. Some promising results were also achieved in seismic monitoring (Fang et al. 2022), loosely coupled GNSS/INS integrated navigation (Xu et al. 2022) and time transfer (Ge et al. 2023).

However, most of these contributions are focused on the accuracy of the PPP-B2b product or PPP performance in a single situation, for example, a permanent station, vehicle experiment, or ship experiment, while knowledge of the performance in airborne applications is still limited. We comprehensively review the PPP-B2b performance in different applications, including static station, car, vessel and aircraft. We first introduce the BDS-3 PPP-B2b correction parameters and the real-time PPP model, highlighting some details not mentioned in previous works. The positioning performance of a real-time kinematic PPP in different situations is sequentially evaluated, discussed, and compared with the existing literature. A summary is finally provided.

Methodology

This section first introduces the user algorithms of applying PPP-B2b corrections, including the precise ephemeris recovery procedure and the datum of PPP-B2b orbit and clock products. Then, the real-time PPP model using PPP-B2b corrections is presented, with special emphasis on the BDS satellite phase center error model.

PPP-B2b correction parameters

Satellite orbit corrections, clock offset corrections, and DCB are essential products broadcasted by B2b signals. Currently, the orbit and clock corrections for GPS and BDS are accompanied with the DCB for BDS only (CSNO 2020a) to correct code biases between inter-frequency and intra-frequency pseudoranges (Hakansson et al. 2017). Since BDS broadcasts multi-frequency signals, including the legacy B1I and B3I signals and the new B1C, B2a and B2b signals, the PPP-B2b DCB corrections contain multiple types, such as B1I-B3I, B1C-B3I, B2a-B3I and B2I-B3I. Hence, users are able to exploit multi-frequency real-time BDS PPP supported with these DCB corrections (Jin and Su 2020).

The precise satellite position $\mathbf{X}_{\text{orbit}}$ can be obtained from the following expression:

$$\begin{cases} \mathbf{X}_{\text{orbit}} = \mathbf{X}_{\text{broadcast}} - \delta\mathbf{X} \\ \delta\mathbf{X} = \left[\mathbf{e}_R \ \mathbf{e}_A \ \mathbf{e}_C \right] \cdot \delta\mathbf{O} \\ \mathbf{e}_R = \dfrac{\mathbf{r}}{|\mathbf{r}|}, \mathbf{e}_C = \dfrac{\mathbf{r} \times \dot{\mathbf{r}}}{|\mathbf{r} \times \dot{\mathbf{r}}|}, \mathbf{e}_A = \mathbf{e}_C \times \mathbf{e}_R \end{cases} \tag{1}$$

where $\mathbf{X}_{\text{broadcast}}$ denotes a satellite position calculated from the broadcast ephemeris. Specifically, the broadcast ephemeris to be used for BDS and GPS is the civil navigation (CNAV1) message of the B1C signal and the legacy

navigation (LNAV) message of the L1C/A signal, respectively (CSNO 2020a). $\delta\mathbf{X}$ is then a satellite position correction in the Cartesian coordinate system, $\delta\mathbf{O}$ is a PPP-B2b orbit correction vector, $\mathbf{e}_R$, $\mathbf{e}_A$ and $\mathbf{e}_C$ are direction unit vector for radial, along-track, and cross-track correction components, and $\mathbf{r}$ and $\dot{\mathbf{r}}$ are the satellite position and velocity vector calculated from the broadcast ephemeris.

The precise satellite clock t_{clock} can be obtained by

$$t_{\text{clock}} = t_{\text{broadcast}} - \frac{C_0}{c} \tag{2}$$

where $t_{\text{broadcast}}$ denotes a satellite clock estimated from broadcast ephemeris, C_0 is a clock correction, and c is the velocity of light in vacuum.

It should be noted, corrected with the PPP-B2b products, satellite precise orbits and clocks correspond to the antenna reference point (ARP), and it is consistent with the datum of frequency of broadcast ephemeris, which is B3I for BDS and IF combination of C1W and C2W for GPS.

The expression for applying the DCB is defined as

$$\tilde{l}_{sig} = l_{sig} - DCB_{sig} \tag{3}$$

where l_{sig} and $\tilde{l}_{sig}$ are pseudorange with and without correcting DCB value (DCB_{sig}). As mentioned before, DCB corrections are not yet provided for GPS. If GPS pseudoranges are not in accordance with the datum of GPS broadcast ephemeris, these require applying of either the inter-signal corrections (ISC) from the new GPS CNAV message (Feess et al. 2013; Steigenberger et al. 2015) or the DCB from any IGS analysis center. In our work, the ISC from GPS CNAV message are used.

Real-time PPP model using PPP-B2b corrections

The dual-frequency IF combinations of GNSS pseudorange and phase observations can be expressed as follows,

$$\begin{cases} P^s_{r,IF} = \rho^s_r + \left(dt_{r,IF} - dt^s_{IF}\right) + \left(d_{r,IF} - d^s_{IF}\right) + Tr^s_r + \varepsilon^s_{r,IF,P} \\ L^s_{r,IF} = \rho^s_r + \left(dt_{r,IF} - dt^s_{IF}\right) + \left(b_{r,IF} - b^s_{IF}\right) + Tr^s_r + \lambda_{IF} N^s_{r,IF} + \varepsilon^s_{r,IF,L} \end{cases} \tag{4}$$

where $P^s_{r,IF}$ and $L^s_{r,IF}$ denote pseudorange and phase IF observations, respectively, ρ^s_r represents a satellite-to-receiver geometric distance with subscripts r for a receiver and s for a satellite, $dt_{r,IF}$ and dt^s_{IF} are receiver and satellite clock offsets, $d_{r,IF}$ and d^s_{IF} are the receiver and satellite hardware delays of the pseudorange IF combination, $b_{r,IF}$ and b^s_{IF} are hardware delays of the phase IF combination, Tr^s_r is the tropospheric delay, λ_{IF} refers to the wavelength of L1 or B1, $N^s_{r,IF}$ is the IF ambiguity, $\varepsilon^s_{r,IF,L}$ and $\varepsilon^s_{r,IF,P}$ is the observation noise for $P^s_{r,IF}$ and $L^s_{r,IF}$, respectively. Any other errors, such as phase wind-up, relativistic effects, and tide displacement, have been corrected with precise models.

The datum of BDS broadcast clock offset aligns with the B3I signal; thus, the satellite clock offset calculated from (2) still contains pseudorange hardware delay of the B3I signal. The DCB correction is required to implement a full consistency of the broadcast ephemeris datum for BDS3 satellites. Considering $dt^s_{IF} + d^s_{IF} = dt^s_{B3I} + \left(d^s_{IF} - d^s_{B3I}\right)$, and assuming we use the B1I/B3I IF combination, we can obtain

$$d^s_{IF} - d^s_{B3I} = f^2_{B1I} \cdot \frac{DCB_{B1I-B3I}}{f^2_{B1I} - f^2_{B3I}} \tag{5}$$

where f_{B1I} and f_{B3I} are the frequency of the B1I and the B3I signal, respectively, and the $DCB_{B1I-B3I}$ is from the PPP-B2b product. The observation equations can be then expressed as

$$\begin{cases} P^s_{r,IF} = \rho^s_r + \left(\overline{dt}_{r,IF} - dt^s_{B3I}\right) - f^2_{B1I} \cdot \dfrac{DCB_{B1I-B3I}}{f^2_{B1I} - f^2_{B3I}} + Tr^s_r + \varepsilon^s_{r,IF,P} \\ L^s_{r,IF} = \rho^s_r + \left(\overline{dt}_{r,IF} - dt^s_{B3I}\right) + Tr^s_r + \overline{N}^s_{r,IF} + \varepsilon^s_{r,IF,L} \end{cases} \tag{6}$$

where $\overline{dt}_{r,IF} = dt_{r,IF} + d_{r,IF}$ and $\overline{N}^s_{r,IF} = \lambda_{IF} N^s_{r,IF} + b_{r,IF} - d_{r,IF} - b^s_{IF} + d^s_{B3I}$ are user-estimated receiver IF pseudorange delay and IF phase ambiguity, respectively, and dt^s_{B3I} is the recovered BDS satellite clock offset. Additionally, the inter-system biases (ISB) should be estimated if multi-GNSS observations are used (Zuo et al. 2021).

It is necessary to note that the phase center offsets (PCO) and phase center variations (PCV) for BDS satellites should be corrected by using the model released by the BDS authority when PPP is implemented based on PPP-B2b products (https://www.beidou.gov.cn/).

SISRE evaluation

The accuracy assessment of the PPP-B2b corrections is conducted before evaluating the PPP performance in various situations. We use the SISRE as an accurate indicator of the PPP-B2b corrections. It is a statistical uncertainty due to errors in satellite orbit and clock product and a key performance indicator for the comparison of different GNSS (Montenbruck et al. 2015). The SISRE can be calculated as follows

$$\text{SISRE} = \begin{cases} \sqrt{(0 \cdot 98 \cdot R - Clk)^2 + \frac{1}{49}\left(A^2 + C^2\right)} & GPS \\ \sqrt{(0 \cdot 99 \cdot R - Clk)^2 + \frac{1}{126}\left(A^2 + C^2\right)} & BDS(GEO/IGSO) \\ \sqrt{(0 \cdot 98 \cdot R - Clk)^2 + \frac{1}{54}\left(A^2 + C^2\right)} & BDS(MEO) \end{cases} \tag{7}$$

where R, A, and C denote orbit errors in radial, along and cross directions in meter, and Clk represents a satellite clock error in meter.

We used the post-processing multi-GNSS products (GBM) provided by GeoForschungsZentrum Potsdam (GFZ) (Deng et al. 2017) as a reference for evaluating the BDS PPP-B2b orbit and clock corrections during the test period. The GBM products are in the IGb14 framework, while BDS employs the CGCS2000 framework. The differences between the two frameworks are negligible compared to the centimeter-level accuracy of the PPP-B2b products, so ignored. And PCO was corrected with the model released by IGS for keeping consistency with the GBM products. The SISRE RMS and STD were calculated for all satellites, first on a daily basis and second as averages over the entire test period.

Figure 1 shows the SISRE RMS and STD of the PPP-B2b product from April to October 2022, i.e., covering the period of all the test cases in our work. The gaps in Fig. 1 are due to receiver failures; hence, data are not available for the statistics. After removing a small number of outliers (6% for GPS) clearly observed in Fig. 1, the SISRE RMS is 0.48 m, 0.76 m and 0.82 m for BDS MEO, IGSO and GPS satellites, respectively, and the corresponding SISRE STD is 0.29 m, 0.44 m and 0.52 m. Some outliers close to 3 m can be observed for GPS SISRE RMS, attributed mainly to the low accuracy (up to 6 ns) of PPP-B2b satellite clock offsets during these days. On the other hand, no outliers are observed for the BDS SISRE. Overall, the errors of the PPP-B2b corrections are approximately by a factor of two larger for GPS compared to BDS and less stable too. The results agree with conclusions from previous works (Tao et al. 2021; Zhang et al. 2022). The smaller errors in the regional network are attributed to inter-satellite links available within the BDS system (Yang et al. 2020). In PPP processing, we thus use a weighting strategy for BDS and GPS in accordance with the SISRE results.

Positioning performance of real-time kinematic PPP

We used a variety of platforms, including permanent stations, car, offshore vessel, and flying aircraft, to evaluate real-time PPP-B2b performance at a user side. BDS and GPS observations from daily files were processed in a simulated real-time mode along with the PPP-B2b corrections recorded by a receiver. The data processing strategy is summarized in Table 1.

Permanent station experiment and results

We used 30-s observations collected at four stations (BJF1, KUN1, LHA1 and SHA1) from the international GNSS monitoring and assessment system (iGMAS) and one station (JFNG) from the IGS multi-GNSS experiment (MGEX) from April 18 to 24, 2022. The reference positions were extracted from the final solutions on April 21, 2022, provided in the software independent exchange format (SINEX) released by iGMAS and IGS, respectively. We defined the PPP convergence time as an interval before reaching the position error smaller than 0.2 and 0.4 m for the horizontal and vertical components, respectively, for 10 continuous

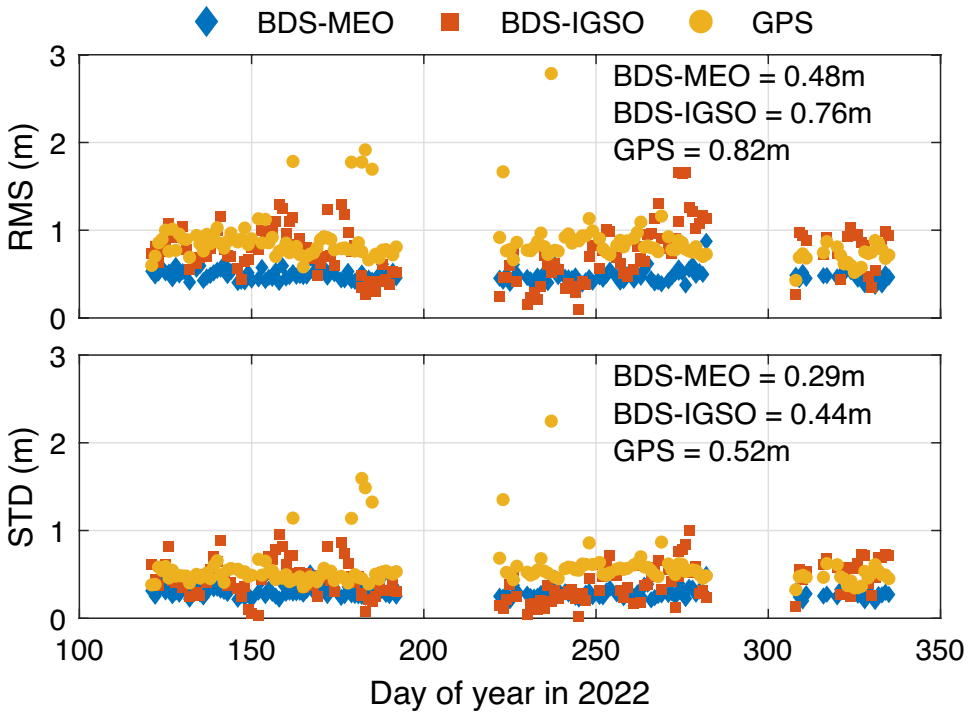

Fig. 1 SISRE RMS and STD of PPP-B2b corrections for GPS, BDS MEO and BDS IGSO satellites from April to October 2022

Table 1 Processing strategy for real-time PPP

Item	Correction model or estimation strategy
Observations	Ionosphere-free linear combination of L1/L2 for GPS and B1I/B3I for BDS
Elevation cutoff	7°
Observations weighting strategy	Elevation-dependent: 1 for elevation (E) > 30°, otherwise 2*sin(E) A-priori sigma: 3 mm and 0.5 m for phase and code observation Weight ratio is 1:2 for GPS and BDS satellites, and 1:2 for IGSO and MEO of BDS satellites
Satellite orbit and clock offsets	B1C CNAV1 broadcast ephemeris for BDS and LNAV broadcast ephemeris for GPS + PPP-B2b corrections
Satellite DCB	PPP-B2b DCB corrections for BDS; CAS DCB products (Wang et al. 2016) for GPS if needed
Satellite PCO/PCV	igs14.atx (Schmid et al. 2016) for GPS; antenna file provided by the BDS authority for BDS
Phase windup	Model corrected
Relativistic effect	Model corrected
Tide model	Solid tide; Polar tide; Ocean tide (Petit and Luzum 2010))
Ionosphere	Eliminated by IF combination
Troposphere	Zenith hydrostatic delay (ZHD) is corrected by GPT3 (Landskron and Bohm 2018) and Saastamoinen model (Saastamoinen 1972); mapping function is GPT3; Zenith wet delay (ZWD) is estimated as a random walk with the process noise of $5mm/\sqrt{h}$
Receiver PCO/PCV	igs14.atx for GPS; use GPS values for BDS if corresponding values are not provided
Receiver clock	Estimated as white noise
ISB	Estimated as a random walk with the process noise of $5mm/\sqrt{h}$
Receiver position	Epoch-wise parameter without constrains between epochs
Ambiguity	Float

minutes at least. An accuracy indicator was the 95% smallest ranked epoch-wise position error excluding the period needed for the convergence.

Figure 2 shows kinematic position errors of real-time PPP using the PPP-B2b corrections for BJF1 and JFNG stations on April 21, 2022. Similar results are obtained for other days too; however, the presented day facilitates a comparison with the results of car experiments. The results reveal that a kinematic PPP converges quickly to the decimeter level for both BDS and BDS + GPS. All positioning errors remain within 40 cm in both N (north), E (east) and U (up) components after the convergence, and the stability of BDS + GPS results outperforms BDS-only. The average horizontal and vertical position accuracy in Fig. 2 is 10.6 cm and 14.2 cm for BDS compared to 8.3 cm and 12.2 cm for BDS + GPS combined solutions.

In Fig. 2, we notice a small jump in the results shortly before 9:00. Since it occurs at all stations at the same time, we attribute it to the PPP-B2b corrections. Hence, we analyze in detail the PPP-B2b orbit and clock offsets on that day (April 21, 2022) in Fig. 3. The error time series of the radial orbit component and the clock offset are normal, but dispersions of along-track and cross-track orbit errors are high and suddenly reduced at about 9:00, while SISRE also exhibits a small jump. This change occurs for all visible BDS satellites; hence, we consider it caused a small jump in the position time series. We are unable to explain this issue further and we can only attribute it to a problem on the provider side.

To further analyze the convergence performance of the real-time PPP based on PPP-B2b corrections, the daily observations are divided into 43 segments with a length of 3 h and a moving step of 30 min, resulting in 1505 segments in total for the test period. The average convergence time of these samples is 28.5 and 12.9 min for BDS-only and BDS + GPS, respectively. The 95% errors for BDS solution after convergence are 19.7 and 21.7 cm in the horizontal and vertical components, respectively, while 13.4 cm and 16.2 cm for BDS + GPS. It can be found that the dual-constellation solution converges faster with smaller errors than standalone BDS. Due to a different accuracy indicator, there are some differences in our results compared to Xu et al. (2021) who reported the average RMS 11.0 and 16.8 cm for BDS-only horizontal and vertical positioning errors, respectively. But the accuracy is close to each other.

Car experiment and results

The car experiment was conducted near the BJF1 station (Beijing, China) on April 21, 2022, the same day as the results in Fig. 2, with a duration of 90 min and a sampling rate of 1 s. The observations were collected by a SOUTH RT300 GNSS receiver with a Harxon HX-CSX049A antenna. The speed of the car was within 10 km/h. The positioning accuracy and convergence time were analyzed similarly to the static experiment. The real-time kinematics (RTK) solution was used as a reference trajectory.

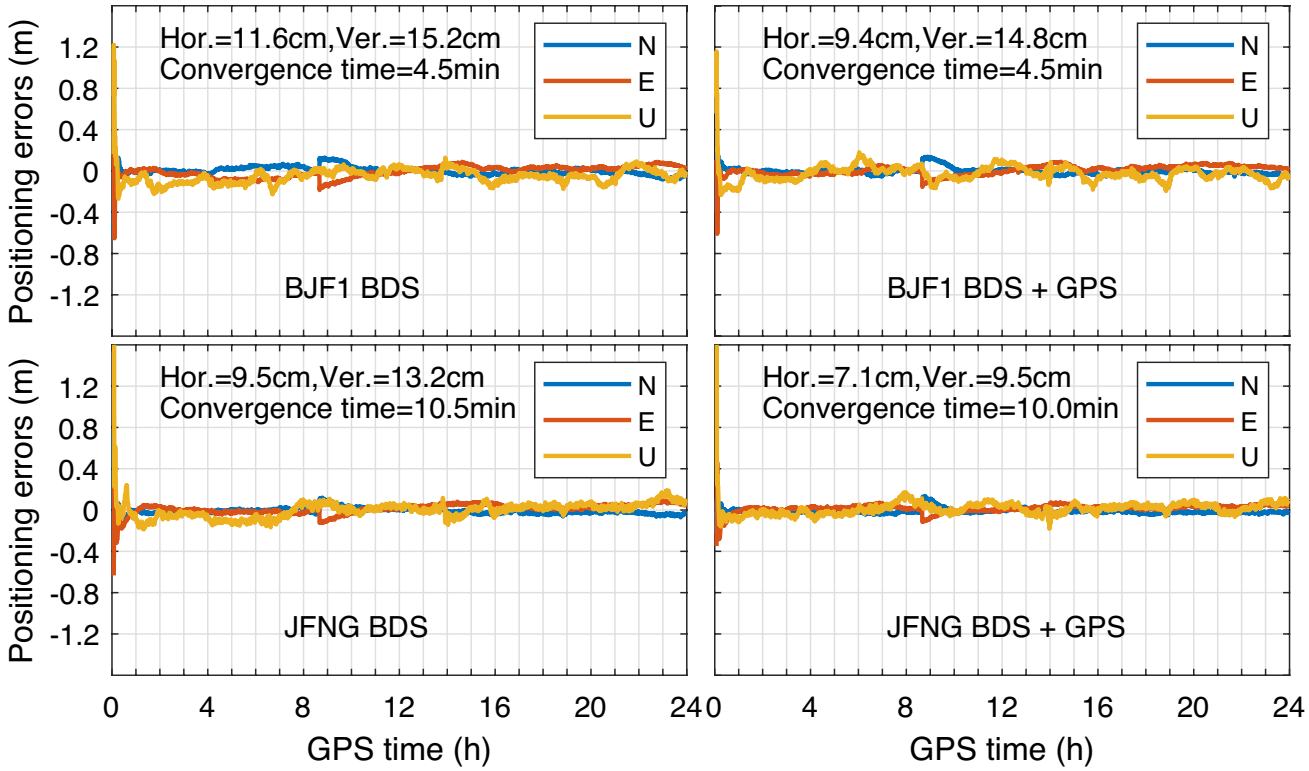

Fig. 2 BDS (left) and BDS + GPS (right) positioning errors of real-time kinematic PPP using PPP-B2b corrections for BJF1 (top) and JFNG (bottom) station on April 21, 2022

The car trajectory and the location of the RTK base station are shown in Fig. 4 (left panel). The length of the RTK baseline is less than 6000 m, and the RTK fix rate is 99.9% and the unfixed RTK results are removed. The number of satellites in the car test period is shown in Fig. 4, with the average number of visible BDS and GPS satellites of 7.1 and 5.8, respectively.

Figure 5 shows time series of kinematic positioning errors in car experiment. The accuracy of a standalone BDS PPP is 11.2 and 17.4 cm in the horizontal and vertical components, respectively, with a convergence time of about 5.1 min. For BDS + GPS PPP, it is 10.6 and 16.6 cm and the convergence time is approximately 4.3 min. The accuracy and the convergence time of the dual-constellation outperform a standalone one (BDS). Car and station positioning experiments yielded similar performances, both coming from the same day.

Offshore vessel experiment and results

The offshore real-time PPP experiment with the BDS PPP-B2b corrections was conducted in the surrounding sea areas of Dongying City, Shandong Province, China. The experiment period lasted from 4:20:00 to 8:00:00 (GPS time) on October 22, 2022, with the speed of the ship within 20 km/h. The antenna was mounted on the top of the cockpit of a fishing boat, as shown in Fig. 6, and the BDS and GPS observations were collected with a sampling rate of 1 s by Sino K803 GNSS module with a VLG GNSS-R44QH antenna.

The RTK solution is taken as a reference again; the ship trajectory and the RTK base station are shown in Fig. 7 (left panel). The distances of the RTK baseline are less than 3500 m, the RTK fix rate is 99.9%, and the unfixed RTK results are removed. The number of satellites in the offshore experiment period is shown in Fig. 7, with the average number of visible BDS and GPS satellites of 7.8 and 4.2, respectively.

The positioning errors from real-time PPP with the BDS PPP-B2b corrections are shown in Fig. 8. The accuracy for BDS PPP is 12.7 and 25.1 cm in the horizontal and vertical components, respectively, with a convergence time of about 29.0 min. For BDS + GPS PPP, it is 10.8 and 21.0 cm, and the convergence time is approximately 6.1 min. The positioning accuracy as well as the convergence time is improved with the inclusion of GPS satellites. Conspicuous fluctuations remain before the convergence in time series of the positioning error of the standalone BDS solution; however, this fluctuation is eliminated after including GPS satellites, indicating that dual-constellation can accelerate the convergence. A

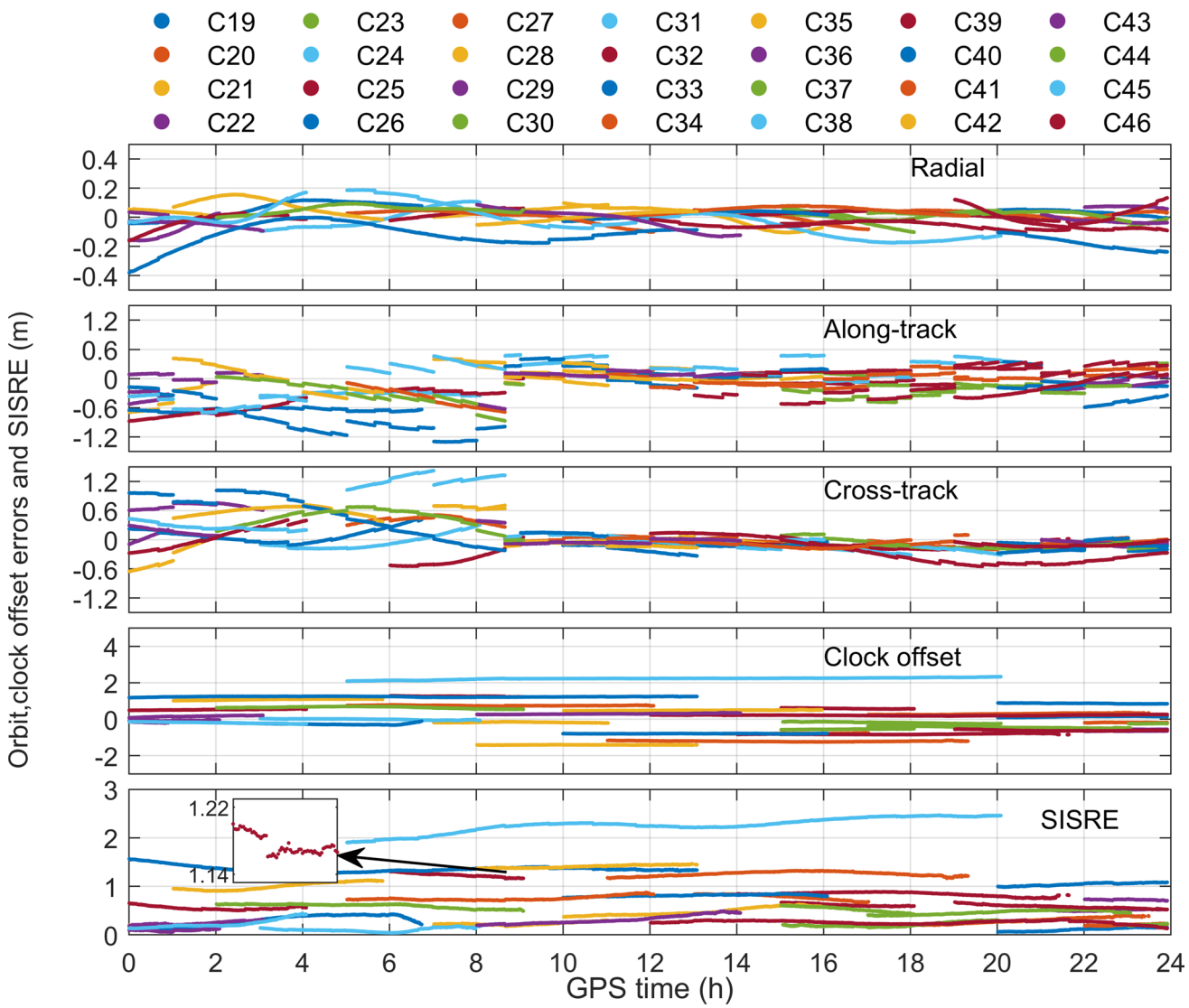

Fig. 3 Error time series of the PPP-B2b real-time orbits, clock offsets and SISRE for the BDS satellites on April 21, 2022 (the subplot in the SISRE panel represents the SISRE time series for satellite C25 between 8:30—9:00)

similar improvement in the vertical direction can also be observed in Geng et al. (2022).

Unmanned aircraft experiment and results

In addition to the experiments described above, we also carried out an aircraft experiment on July 24, 2022, with a duration of about 4 h and a sampling rate of 0.1 s (HI-TARGET K20 receiver and AT-35101 antenna). The reference trajectory was processed using the RTK method (CHCHAV P5 receiver and HX-CSX627A antenna), the GBM post-processing products (Deng et al. 2017), and the Inertial Explorer (IE) software by the Novatel company (https://novatel.com). The RTK reference was not fixed solutions. However, the software provided three-dimensional (3D) STD as coordinate accuracy indicators. The percentage of RTK references whose 3D STD was better than 4 cm was about 92%, between 4 and 6 cm, about 7.7%, and above 6 cm, about 0.3%. In order to match the RTK reference, the raw observations were re-sampled to 1 s.

Figure 9 displays a brief trajectory of the aircraft in the experiment. We can see that the aircraft ascends fast at the beginning (GPST 4.0—4.4 h), then horizontally flies to the southeast direction (4.4—5.5 h) and descends (5.5—5.8 h), finally keeps a quasi-rectangle trajectory of ten strips (5.8—7.8 h). The aircraft's velocity is about 230 km/h in the experiment period. The baseline length of RTK gradually decreases from 400 to 20 km over time.

According to the characteristics of aircraft trajectory, we optimize the process noise of zenith tropospheric delay

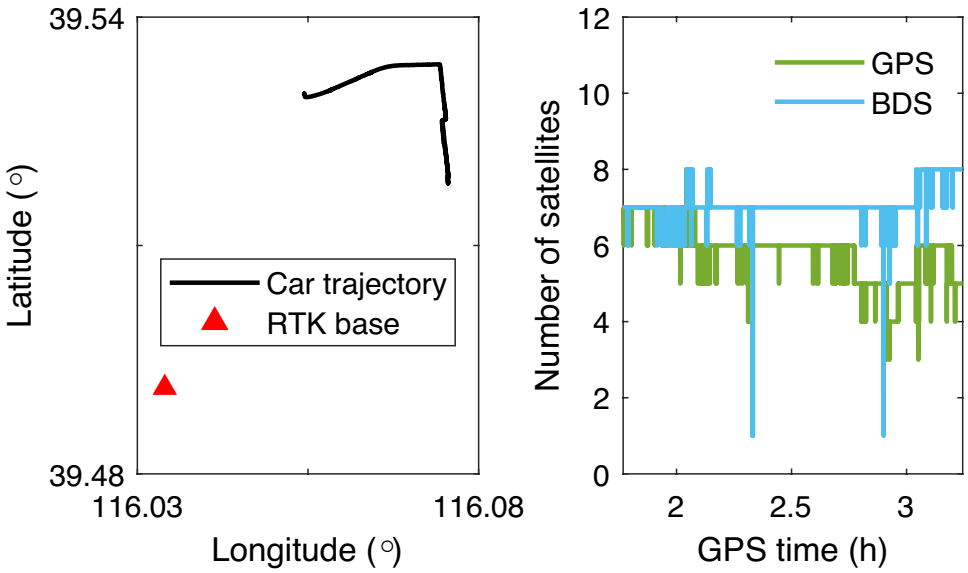

Fig. 4 Car trajectory and location of RTK base station (left) and number of visible satellites (right)

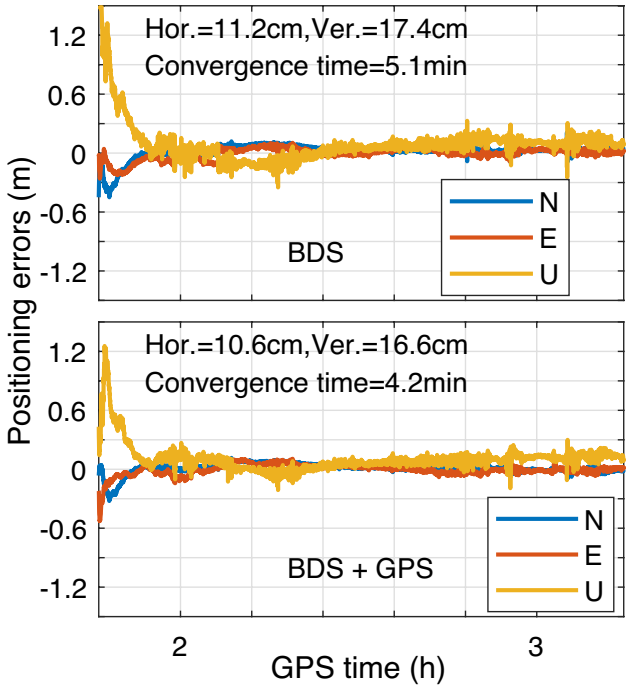

Fig. 5 BDS-only (top) and BDS + GPS (bottom) real-time kinematic PPP positioning errors for car experiment

(ZTD) to adapt the fast attitude change. First, we extract the time and coordinates of the beginning and end point of the ascending and descending phases. Second, the ZTD at the corresponding position and moment is calculated by NWMs-based Site module of GMET Online Service (http://gmet.users.sgg.whu.edu.cn/). Then, it is possible to calculate the process noise of ZTD in these two stages using the expression in Hadas et al. (2017). Eventually, the process noise of ZTD is set to 15 cm/$\sqrt{\text{h}}$ when the aircraft is climbing and descending and maintained at 5 mm/$\sqrt{\text{h}}$ when the aircraft is leveling.

Figure 10 shows the positioning errors and the height of the aircraft. The accuracy of the BDS and BDS + GPS PPP is 18.1 (32.8) cm and 17.1 (31.3) cm in the horizontal (vertical) direction, respectively, and the convergence time is approximately 48.9 and 43.1 min. In Fig. 10, we can clearly see how the altitude of the aircraft changes over time. The aircraft ascends fast to the altitude of 2000 m and after about an hour, descends to an altitude of about 500 m and, finally, maintains this altitude until the end of the experiment.

In Fig. 10, visible undulation is present in both BDS and BDS + GPS combined solutions during the flight in strips, and the positioning error varies sharply during the period when the aircraft is maneuvering between adjoining strips.

Fig. 6 Receiver antenna and environment for offshore real-time positioning experiment

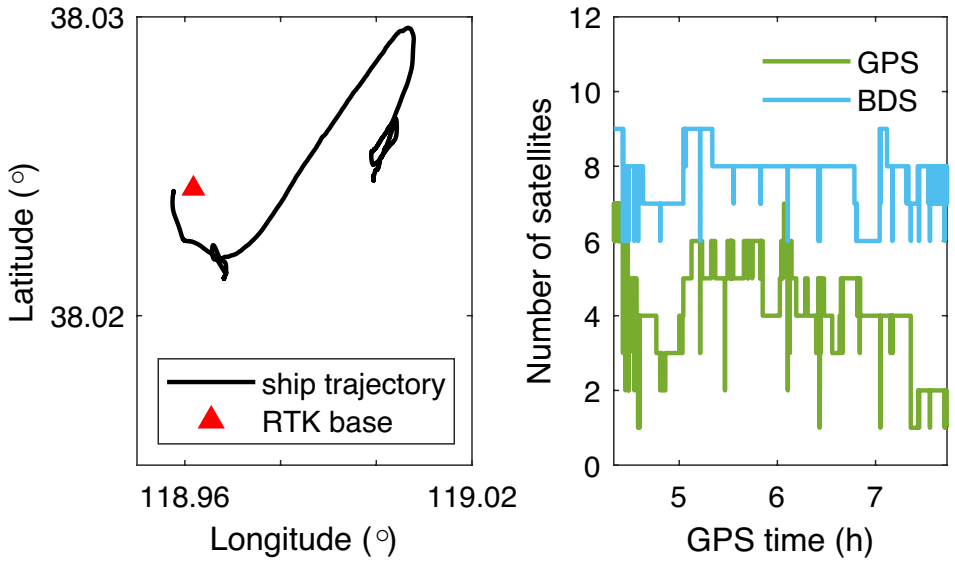

Fig. 7 Ship trajectory and location of RTK base station (left) and number of visible satellites (right)

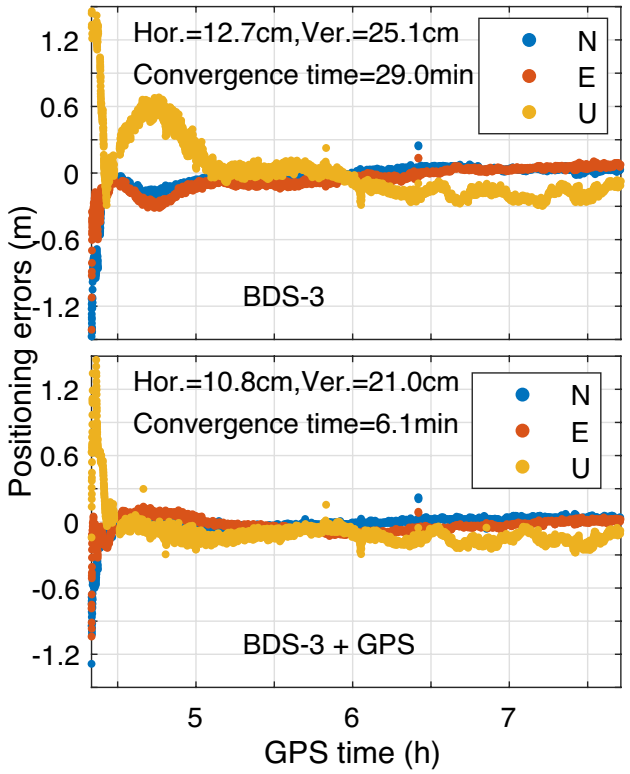

Fig. 8 BDS-only (top) and BDS + GPS (bottom) real-time kinematic PPP positioning errors for offshore experiment

A similar coordinate error pattern in airborne platforms is also discovered by Shi et al. (2017), Grayson et al. (2018), Shi et al. (2020) and Ocalan et al. (2022). Therefore, we consider it as a normal error in the GNSS-driven positioning of the airborne platform, and it is logically independent on the PPP-B2b corrections. In PPP-supported aerial triangulation, Shi et al. (2017) utilized three translation and three drift parameters to compensate this strip-dependent coordinate error, and a satisfactory improvement is obtained. However, in post-processing mode, this compensation method is mainly purposed to eliminate the effect of systematic errors induced by GNSS positioning on the perspective center of the aerial camera in aerial triangulation. Therefore, we do not intend to compensate for this strip-dependent undulation in our simulated real-time PPP result.

The number of satellites of BDS and BDS + GPS and corresponding position dilution of precision (PDOP) are shown in Fig. 11. During the approximate 4-h period, the average PDOP and number of satellites of single BDS are 9.3 and 7.9, respectively. Dual-constellation then provides an average PDOP of 3.8 and number of satellites of 12.3. The convergence time for the aircraft is significantly longer than that of the other experiments. In Fig. 11, we notice two spikes in PDOP series at about 4.1 h and 4.4 h induced by the change in the number of satellites. Both two fast changes appear during the convergence and the PDOP changes frequently before the second spike (at about 4.4 h). These two reasons can explain the relatively longer convergence time for the aircraft experiment.

Discussions

To compare the results in different platforms, we summarize the accuracy and the convergence time of all the positioning experiments in Table 2. The positioning accuracy is generally consistent with the official declaration of the positioning error at a decimeter level for the kinematic mode when using the BDS PPP service (CNSO 2020b).

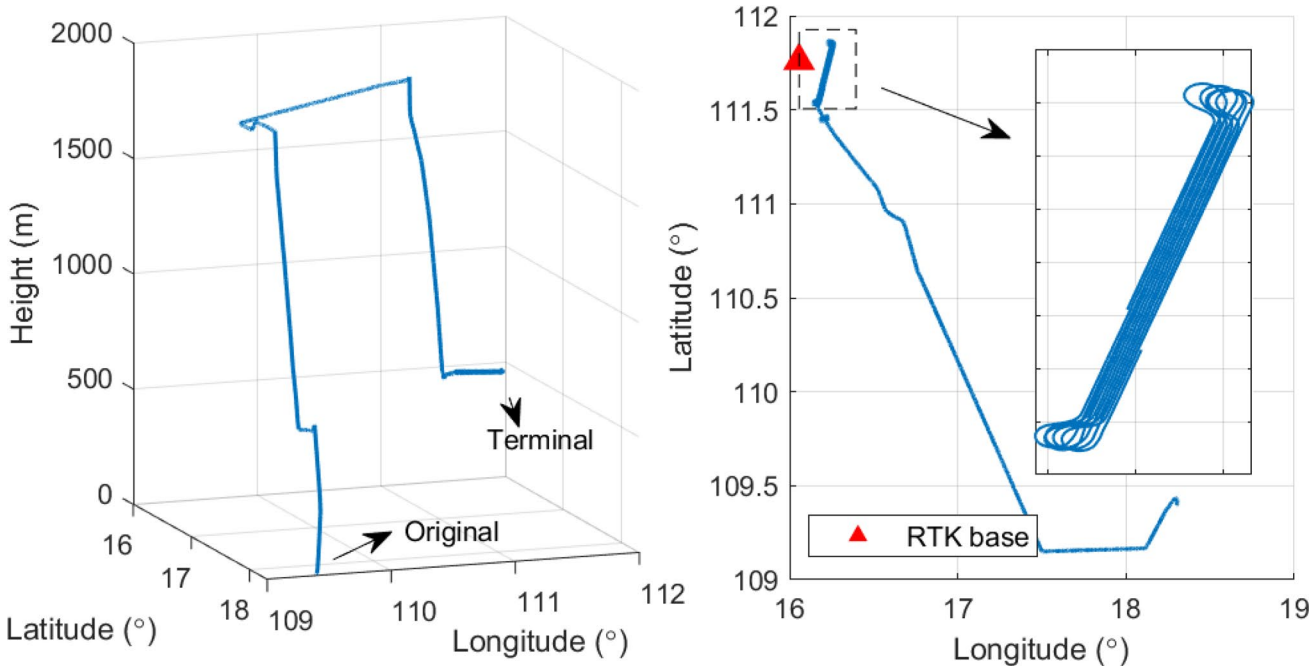

Fig. 9 Aircraft trajectory in three-dimensional diagram (left), and in latitude and longitude (right)

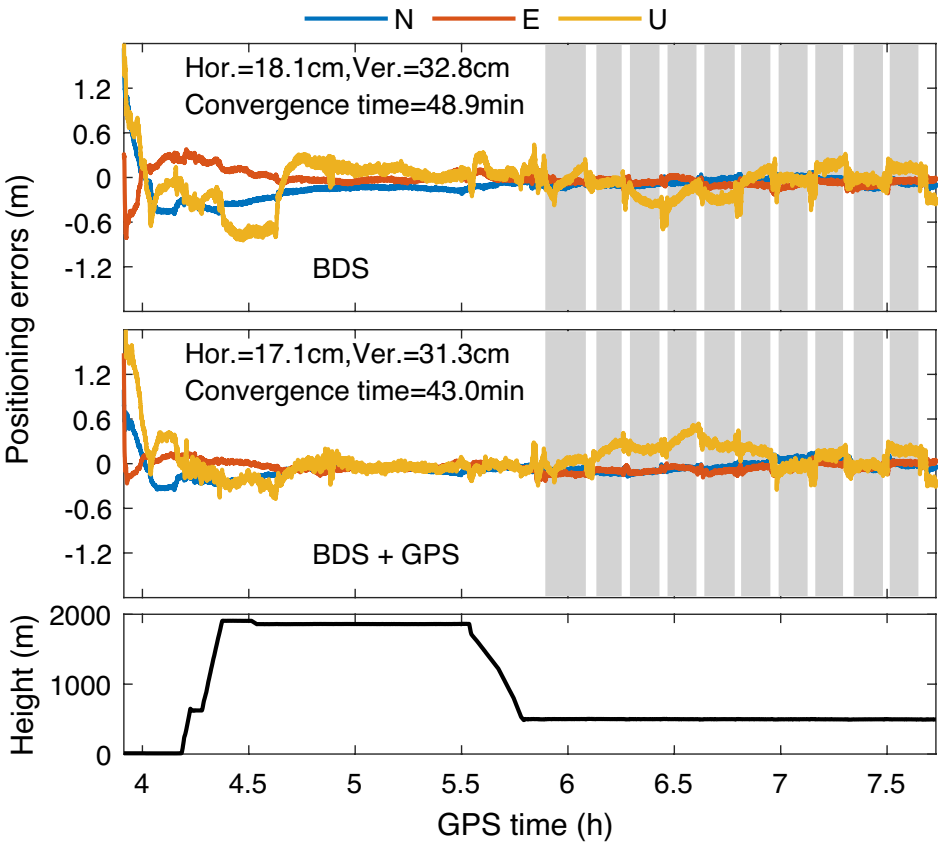

Fig. 10 BDS-only (top), the BDS + GPS (middle) kinematic PPP positioning errors for the aircraft experiment. The height of the aircraft is shown at the bottom. The gray backgrounds are adopted to identify ten strips

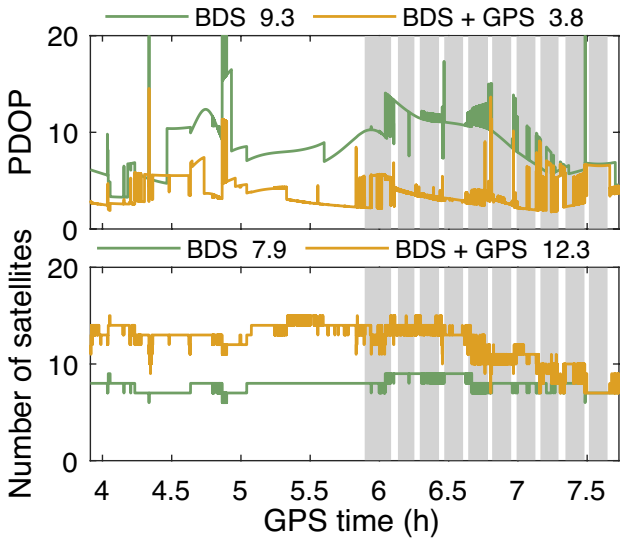

Fig. 11 PDOP (top) and number of satellites (bottom) in aircraft experiment. The gray backgrounds are adopted to mark ten strips

The permanent station, car and offshore vessel, which all can be classified as static or low kinematic platforms, achieves a similar performance in terms of positioning accuracy. The positioning errors after convergence at the 95% confidence level are generally superior to 20 cm in horizontal directions and 26 cm in vertical directions. However, the high kinematic airborne PPP experiment results in slightly worse positioning accuracy and significantly longer convergence time, but still with an error of less than 20 and 35 cm in the horizontal and vertical directions, respectively. A relatively poor accuracy of the aircraft is attributed to the strip-dependent pattern error. Due to the limited duration of observations in the vehicle experiment, the convergence time in Table 2 is indicative requiring a careful interpretation.

Regarding the comparison between BDS-only and BDS + GPS PPP, the latter generally outperforms the former. After including additional constellation, the convergence is shortened considerably (by more than 70%), as shown in the offshore vessel experiment. While as it concern positioning error, due to our choice of a 95% error as the accuracy indicator, the improvements in horizontal and vertical are in the range of 4.6% (vertical component in car and aircraft experiment) and 32.0% (horizontal component in permanent station experiment).

Conclusions

The BDS PPP service provides a promising opportunity for exploiting real-time PPP for GNSS users in China and surrounding areas. This featured service will also have great potential in environments without a stable Internet network.

We present a comprehensive evaluation of the kinematic PPP performance of the PPP-B2b service in different situations. The statistical results of seven days of observations at five permanent stations indicate that the average convergence time is 28.5 min for standalone BDS, and 12.9 min for BDS + GPS. In terms of accuracy, represented by the 95% positioning errors after the convergence, the BDS solution using the B1I/B3I IF combination achieves 19.7 cm in the horizontal directions and 21.7 cm in the vertical. For BDS + GPS combined solutions, the accuracy is 13.4 and 16.2 cm in horizontal and vertical directions, respectively.

Similarly, the PPP car experiment exhibits an accuracy of 11.2 (10.6) and 17.4 (16.6) cm in the horizontal and vertical direction, respectively, with a convergence of 5.1 (4.3) min for BDS (BDS + GPS) solution. The accuracy of the offshore positioning is 12.7 (10.8) and 25.1 (21.0) cm in horizontal and vertical components after a convergence of 29.0 (6.1) min. The aircraft-based PPP experiment, however, results in a positioning accuracy of 18.1 cm in horizontal and 32.8 cm in vertical components after a convergence time of 48.9 min for BDS-only. When combining BDS and GPS, the average positioning accuracy becomes 17.1 and 31.3 cm in horizontal and vertical directions, respectively, i.e., without significant improvements compared to the BDS accuracy, while the convergence time decreases to 43.1 min. Thus, airborne positioning results become slightly worse compared to low kinematic vehicle experiments.

The achieved positioning accuracies from different experiments are consistent with the official declaration of the positioning errors for the BDS-B2b service, i.e., to support a decimeter level. In future, the PPP services of other GNSS

Table 2 95% positioning error (after convergence), convergence time for the real-time kinematic experiment, and improvements of BDS + GPS results compared to BDS.

	BDS / BDS + GPS			Improvement rate (dual-constellation)		
	Horizontal[cm]	Vertical[cm]	Convergence Time [min]	Horizontal[%]	Vertical[%]	Convergence Time [%]
Permanent station	19.7 / 13.4	21.7 / 16.2	28.5 / 12.9	32.0	25.6	54.7
Car	11.2 /10.6	17.4 / 16.6	5.1 / 4.2	5.4	4.6	17.6
Offshore vessel	12.7 / 10.8	25.1 / 21.0	29.0 / 6.1	15.0	16.3	79.0
Aircraft	18.1 / 17.1	32.8 / 31.3	48.9 / 43.0	5.5	4.6	12.1

systems, such as Galileo and QZSS, will be available too, which will further improve the positioning performance of the satellite-based real-time PPP and promote the application of real-time PPP in more fields.

Acknowledgements This work is supported by the National Key Research and Development Program of China (Grant 2021YFC3000501), the National Natural Science Foundation of China (Grant 42174027), the Fundamental Research Funds for the Central Universities (Grant 2042022kf1198), and the Young Elite Scientist Sponsorship Program by CAST(YESS20200110).

Author contributions Conceptualization: Peida Wu, Yidong Lou, Weixing Zhang; Formal analysis and investigation: Peida Wu; Writing - original draft preparation: Peida Wu; Writing - review and editing: Yidong Lou, Weixing Zhang, Jan Dousa; Funding acquisition: Yidong Lou, Weixing Zhang; Resources: Yidong Lou, Weixing Zhang, Huizhong He, Junbing Chai, Yongzhong Ouyang, Zhenyi Zhang, Xu Zou; Supervision: Yidong Lou, Weixing Zhang.

Data availability The GNSS data of MGEX station were obtained from https://cddis.nasa.gov/archive/gnss/data/daily/, and the GBM products were accessed from https://dataservices.gfz-potsdam.de. The GNSS results that support the findings are available at https://github.com/YoYogurt/B2b_evaluation_paper. The GNSS dataset of the car and offshore ship is available upon request.

Declarations

Competing interests The authors declare no competing interests.

References

Booth JS, Snow RN (2009) An evaluation of OmniStar XP and PPP as a replacement for DGPS in airborne applications. Proceedings of ION GNSS 2009, Institute of Navigation, Savannah, Georgia, USA, September 22–25, 1188–1194.

Cabinet Office, Government of Japan, 2022. Trial service of MADOCA-PPP has now started [EB/OL]. https://qzss.go.jp/en/overview/notices/madoca_220930.html

CSNO (2020a). BeiDou Navigation Satellite System Signal in Space Interface Control Document Precise Point Positioning Service Signal PPP-B2b (Version 1.0). China Satellite Navigation Office. http://www.beidou.gov.cn/xt/gfxz/2020a08/P020200808336206248294 0.pdf

CSNO (2020b). BeiDou Navigation Satellite System Open Service Performance Standard (Version 3.0). China Satellite Navigation Office. http://www.beidou.gov.cn/xt/gfxz/202105/P020210526216231136238.pdf

Dai L, Chen Y, Lie A, Zeitzew M, Zhang Y (2016) StarFire SF3: worldwide centimeter-accurate real time GNSS positioning. Proceedings of ION GNSS 2016, Institute of Navigation, Portland, Oregon, USA, September 12–16, 3295–3320.

Deng Z, Nischan T, Bradke M (2017) Multi-GNSS Rapid Orbit-, Clock- and EOP-Product Series. GFZ Data Services. https://doi.org/10.5880/GFZ.1.1.2017.002

Elsobeiey M, Al-Harbi S (2016) Performance of real-time precise point positioning using IGS real-time service. GPS Solutions 20(3):565–571. https://doi.org/10.1007/s10291-015-0467-z

European GNSS Service Centre (2023). Galileo high accuracy service service definition document (HAS SDD) (Issue 1.0) https://www.gsc-europa.eu/sites/default/files/sites/all/files/Galileo-HAS-SDD_v1.0.pdf

Fang R, Lv H, Hu Z, Wang G, Zheng J, Zhou R, Xiao K, Li M, Liu J (2022) GPS/BDS precise point positioning with B2b products for high-rate seismogeodesy: application to the 2021 M-w 7.4 Maduo earthquake. Geophys J Int 231(3):2079–2090. https://doi.org/10.1093/gji/ggac311

Feess W, Cox J, Howard E, Kovach K (2013) GPS Inter-Signal Corrections (ISCs) Study. Proceedings of ION GNSS 2013, Nashville, Tennessee, USA, September 16–20, 951–958.

Ge Y, Cao X, Lyu D, He Z, Ye F, Xiao G, Shen F (2023) An investigation of PPP time transfer via BDS-3 PPP-B2b service. GPS Solut 27(2):61. https://doi.org/10.1007/s10291-023-01402-y

Geng T, Li Z, Xie X, Liu W, Li Y, Zhao Q (2022) Real-time ocean precise point positioning with BDS-3 service signal PPP-B2b. Measurement 203:111911. https://doi.org/10.1016/j.measurement.2022.111911

Grayson B, Penna NT, Mills JP, Grant DS (2018) GPS precise point positioning for UAV photogrammetry. Photogrammetric Record 33(164):427–447. https://doi.org/10.1111/phor.12259

Hadas T, Bosy J (2015) IGS RTS precise orbits and clocks verification and quality degradation over time. GPS Solut 19(1):93–105. https://doi.org/10.1007/s10291-014-0369-5

Hadas T, Teferle FN, Kazmierski K, Hordyniec P, Bosy J (2017) Optimum stochastic modeling for GNSS tropospheric delay estimation in real-time. GPS Solut 21(3):1069–1081. https://doi.org/10.1007/s10291-016-0595-0

Hakansson M, Jensen ABO, Horemuz M, Hedling G (2017) Review of code and phase biases in multi-GNSS positioning. GPS Solusitons 21(3):849–860. https://doi.org/10.1007/s10291-016-0572-7

Jin S, Su K (2020) PPP models and performances from single- to quad-frequency BDS observations. Satellite Navigation. https://doi.org/10.1186/s43020-020-00014-y

Kouba J, Héroux P (2001) Precise point positioning using IGS Orbit and clock products. GPS Solut 5(2):12–28. https://doi.org/10.1007/PL00012883

Landskron D, Bohm J (2018) VMF3/GPT3: refined discrete and empirical troposphere mapping functions. J Geodesy 92(4):349–360. https://doi.org/10.1007/s00190-017-1066-2

Leandro R, et al. 2011 RTX Positioning: The Next Generation of cm-accurate Real-time GNSS Positioning. Proceedings of ION GNSS 2011, Portland, Oregon, USA, September 20–23, 1460–1475.

Li B, Ge H, Bu Y, Zheng Y, Yuan L (2022) Comprehensive assessment of real-time precise products from IGS analysis centers. Satellite Navigation. https://doi.org/10.1186/s43020-022-00074-2

Liu Y, Yang C, Zhang M (2022) Comprehensive analyses of PPP-B2b performance in china and surrounding areas. Remote Sens. https://doi.org/10.3390/rs14030643

Lou Y, Dai X, Gong X, Li C, Qing Y, Liu Y, Peng Y, Gu S (2022) A review of real-time multi-GNSS precise orbit determination based on the filter method. Satell Navig. https://doi.org/10.1186/s43020-022-00075-1

Malys S, Jensen PA (1990) Geodetic point positioning with GPS carrier beat phase data from the CASA UNO experiment. Geophys Res Lett 17(5):651–654. https://doi.org/10.1029/gl017i005p00651

Montenbruck O, Steigenberger P, Hauschild A (2015) Broadcast versus precise ephemerides: a multi-GNSS perspective. GPS Solut 19(2):321–333. https://doi.org/10.1007/s10291-014-0390-8

Ocalan T, Turk T, Tunalioglu N, Gurturk M (2022) Investigation of accuracy of PPP and PPP-AR methods for direct georeferencing in UAV photogrammetry. Earth Sci Inf 15(4):2231–2238. https://doi.org/10.1007/s12145-022-00868-7

Petit G, Luzum B, 2010. IERS Conventions (2010). Frankfurt am Main: Verlag des Bundesamts für Kartographie und Geodäsie, 2010. 179 pp, ISBN 3–89888–989–6

Ren Z, Gong H, Peng J, Tang C, Huang X, Sun G (2021) Performance assessment of real-time precise point positioning using BDS PPP-B2b service signal. Adv Space Res 68(8):3242–3254. https://doi.org/10.1016/j.asr.2021.06.006

Saastamoinen J (1972) Atmospheric correction for the troposphere and stratosphere in radio ranging satellites. The Use of Artificial Satellites for Geodesy. https://doi.org/10.1029/GM015p0247

Schmid R, Dach R, Collilieux X, Jäggi A, Schmitz M, Dilssner F (2016) Absolute IGS antenna phase center model igs08.atx: status and potential improvements. J Geodesy 90(4):343–364. https://doi.org/10.1007/s00190-015-0876-3

Shi J, Yuan X, Cai Y, Wang G (2017) GPS real-time precise point positioning for aerial triangulation. GPS Solut 21(2):405–414. https://doi.org/10.1007/s10291-016-0532-2

Shi J, Huang Y, Ouyang C, Lu X, Xu C (2020) BeiDou/GPS relative kinematic positioning in challenging environments including poor satellite visibility and high receiver velocity. Surv Rev 52(371):172–182. https://doi.org/10.1080/00396265.2018.1537227

Steigenberger P, Montenbruck O, Hessels U (2015) Performance evaluation of the early CNAV navigation message. Navigation-J Institute of Navigation 62(3):219–228. https://doi.org/10.1002/navi.111

Tao J, Liu J, Hu Z, Zhao Q, Chen G, Ju B (2021) Initial Assessment of the BDS-3 PPP-B2b RTS compared with the CNES RTS. GPS Solut. https://doi.org/10.1007/s10291-021-01168-1

Wang N, Yuan Y, Li Z, Montenbruck O, Tan B (2016) Determination of differential code biases with multi-GNSS observations. J Geodesy 90(3):209–228. https://doi.org/10.1007/s00190-015-0867-4

Xu X, Nie Z, Wang Z, Wang B, Du Q (2022) Performance assessment of BDS-3 PPP-B2b/INS loosely coupled integration. Remote Sens 14(13):2957. https://doi.org/10.3390/rs14132957

Xu Y, Yang Y, Li J (2021) Performance evaluation of BDS-3 PPP-B2b precise point positioning service. GPS Solut. https://doi.org/10.1007/s10291-021-01175-2

Yang Y, Mao Y, Sun B (2020) Basic performance and future developments of BeiDou global navigation satellite system. Satellite Navigation. https://doi.org/10.1186/s43020-019-0006-0

Zhang W, Lou Y, Song W, Sun W, Zou X, Gong X (2022) Initial assessment of BDS-3 precise point positioning service on GEO B2b signal. Adv Space Res 69(1):690–700. https://doi.org/10.1016/j.asr.2021.09.006

Zumberge J, Heflin M, Jefferson D, Watkins M, Webb F (1997) Precise point positioning for the efficient and robust analysis of GPS data from large networks. J Geophys Res-Solid Earth 102(B3):5005–5017. https://doi.org/10.1029/96JB03860

Zuo X, Jiang X, Li P, Wang J, Ge M, Schuh H (2021) A square root information filter for multi-GNSS real-time precise clock estimation. Satellite Navigation. https://doi.org/10.1186/s43020-021-00060-0

Peida Wu received his Master's degree from Central South University in 2018 and is now a doctoral candidate at GNSS Research Center, Wuhan University. His current research mainly focuses on GNSS data processing and tropospheric model refinement in complex environments.

Yidong Lou received his Ph.D. in Geodesy and Surveying Engineering from Wuhan University in 2008 and is currently a professor at GNSS Research Center, Wuhan University. His current research interests are in real-time precise GNSS orbit determination and real-time GNSS PPP.

Weixing Zhang received his Ph.D. in Geodesy and Surveying Engineering from Wuhan University in 2016 and is currently an associate professor at GNSS Research Center, Wuhan University. His research interests include GNSS data processing and GNSS meteorology.

Jan Dousa received his M.Sc. and Ph.D. in geodesy from the Czech Technical University in Prague in 1995 and 1999, respectively. Since 1996, he has worked at Geodetic Observatory Pecny for developing high accuracy GNSS applications, including the determination of precise orbits, modeling and monitoring troposphere, the realization of the reference frame and others. He is a founder and developer of the G-Nut software library and end-user applications.

Huizhong He is currently a senior engineer. He has been long engaged in research and application of marine surveying and marine geophysical engineering.

Junbing Chai received his Master's degree from the China University of Petroleum in 2016. He is currently a senior engineer primarily engaged in the research, development, and application of precision positioning software for GNSS.

Yongzhong Ouyang received his Ph.D. degree from Wuhan University in 2013. He has researched and applied marine gravity field determination theoretical methods.

Zhenyi Zhang received the Master's degree in geodesy and survey engineering from Wuhan University, Wuhan, China, in 2023, and would join ETH Zurich as a Ph.D. student in October 2023. His research interests include GNSS data processing algorithms and applications, GNSS meteorology, numerical weather modeling, and machine learning.

Xu Zou received his B.S. degree from Jianghan University in 2016 and is currently working in GNSS data processing at the GNSS Research Center, Wuhan University.